Characterization of intra-graft B cells during renal allograft rejection

Valeriya Zarkhin[1,4], Neeraja Kambham[2,4], Li Li[1], Shirley Kwok[2], Szu-Chuan Hsieh[1], Oscar Salvatierra[1,3] and Minnie M. Sarwal[1,3]

[1]Department of Pediatrics, Stanford University Medical Center, Stanford, California, USA; [2]Department of Pathology, Stanford University Medical Center, Stanford, California, USA and [3]Department of Surgery, Stanford University Medical Center, Stanford, California, USA

Intra-graft CD20$^+$ B-cell clusters are found during acute rejection of renal allografts and correlate with graft recovery following rejection injury. Here using archived kidney tissue we conducted immunohistochemical studies to measure specific subsets of pathogenic B cells during graft rejection. Cluster-forming CD20$^+$ B cells in the rejected graft are likely derived from the recipient and are composed of mature B cells. These cells are activated (CD79a$^+$), and present MHC Class II antigen (HLADR$^+$) to CD4$^+$ T cells. Some of these clusters contained memory B cells (CD27$^+$) and they did not correlate with intra-graft C4d deposition or with detection of donor-specific antibody. Further, several non-cluster forming CD20$^-$ B-lineage CD38$^+$ plasmablasts and plasma cells were found to infiltrate the rejected grafts and these cells strongly correlated with circulating donor-specific antibody, and to a lesser extent with intra-graft C4d. Both CD20$^+$ B cells and CD38$^+$ cells correlated with poor response of the rejection to steroids. Reduced graft survival was associated with the presence of CD20 cells in the graft. In conclusion, a specific subset of early lineage B cells appears to be an antigen-presenting cell and which when present in the rejected graft may support a steroid-resistant T-cell-mediated cellular rejection. Late lineage interstitial plasmablasts and plasma cells may also support humoral rejection. These studies suggest that detailed analysis of interstitial cellular infiltrates may allow better use of B-cell lineage specific treatments to improve graft outcomes.

Kidney International (2008) **74,** 664–673; doi:10.1038/ki.2008.249; published online 11 June 2008

KEYWORDS: renal allograft rejection; intra-graft CD20$^+$ and CD38$^+$ infiltrates; B-lymphocytes; transplant biopsy; graft survival

Correspondence: *Minnie M. Sarwal, Department of Pediatrics, Stanford University Medical Center, G306, 300 Pasteur Drive, Stanford, California 94304, USA. E-mail: msarwal@stanford.edu*

[4]These authors contributed equally to this work.

Received 1 October 2007; revised 27 March 2008; accepted 1 April 2008; published online 11 June 2008

CD20$^+$ lymphocytic infiltrates have been demonstrated to be potentially pathogenic in transplant cellular acute rejection (AR), correlating with a phenotype of a rejection that is more recalcitrant to conventional treatment, an increased risk of graft loss, and independent of C4d peritubular deposition.[1–6] Other studies have not always shown this clinical correlation,[7–9] and it is unclear if these differences may, in part, be related to the patient group under study with underlying differences secondary to recipient age, the variability of specific transplant center induction and immunosuppression protocols, or because of differences in the specific lineage of CD20$^+$ B cells observed in different types of graft rejection.[1]

Detailed phenotypic analyses of CD20$^+$ B-cell infiltrates in graft rejection have not been performed to date. Given the number of immunohistochemistry stains required to comprehensively phenotype the lineage of infiltrating B cells and the limitation of human renal biopsy tissue available post-diagnostic evaluation, these studies are difficult to perform extensively on patient samples. With this in mind, tissue microarrays using transplant nephrectomies offer the best (if not ideal) alternative to biopsies for screening of possible immunohistochemical (IHC) predictors of graft outcome. Moreover, the transplant nephrectomy patients are often weaned off all immunosuppression prior to surgery, resulting in uninhibited full-blown immunological attack on the allograft. In our study, we have attempted to capture this phenotype of severe AR, utilizing tissue microarray tools, with a focus on the different lineages of infiltrating B cells in graft rejection.

RESULTS

Comprehensive immunostaining was performed initially on kidney tissue microarray (K-TMA) samples and selected, relevant immunostains were then performed in core biopsy samples with rejection, and the results were correlated with specific clinical graft outcomes.

Distinct B-cell lineages in rejecting grafts

Two predominant lineages of B cells were identified at the time of AR (Figure 1a): interstitial CD20$^+$ B-cell clusters and interstitial scattered CD38$^+$ plasmablasts and plasma cells. Fluorescence *in situ* hybridization (FISH) for the X and Y

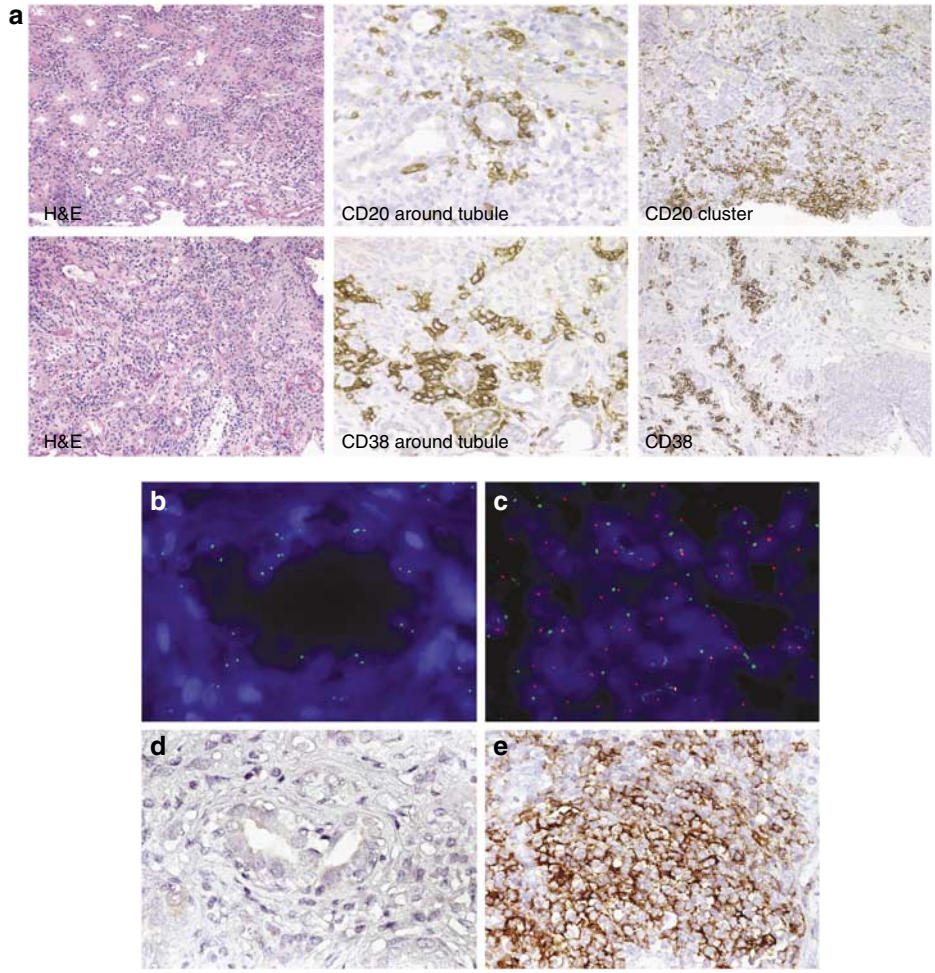

Figure 1 | Different B-cell subsets populate rejecting kidney allografts (a) and these B cells are recipient derived (b–e). (**a**) Two different B-cell subsets are identified in AR: representative renal allograft core biopsies were stained for H&E, CD20, and CD38 markers. Two major nonoverlapping populations of B cells are seen and these include $CD20^+$ but $CD38^-$ cells mostly in clusters (upper panel) and $CD20^-$ but $CD38^+$ interstitial plasmablasts and plasma cells (lower panel, original magnification $\times 200$). The $CD20^+$ and $CD38^+$ cells can be seen in the interstitium, surrounding the tubules, but not causing tubulitis (original magnification $\times 300$). (**b–e**) $CD20^+$ B-cell clusters in rejecting kidney allografts are recipient derived. FISH for X (green signal) and Y (red signal) chromosome probes was performed on all K-TMA cores and a representative core with AR (T-11) from a male recipient of a female donor kidney is shown here (original magnification $\times 400$). CD20 stain and FISH were performed on consecutive sections to be able to locate the B-cell clusters on FISH sections accurately. As shown, the tubule is from a female donor kidney (XX, **b**) and the B-cell clusters seen in the interstitium are likely recipient derived (XY, **c**), although few Y-chromosome-positive cells within the B-cell cluster may also be colocalizing T cells or macrophages. The serial section stained with CD20 is also shown, corresponding to the area of the tubule (**d**) and B-cell cluster (**e**).

chromosomes in sex-mismatched donor and recipient pairs suggests that the B cells in AR were recipient derived (Figure 1b–e).

$CD20^+$ clusters. As elucidated by the K-TMA immunostains, the $CD20^+$ B-cell clusters were of early lineage, with an activated phenotype, with positive staining for CD79a. Few, but not all cluster cells positive for CD20 and negative for CD3, expressed the CD27 marker, suggesting that B-cell clusters contain some memory B cells (Figure 2a; Figure S3). B-cell clusters also stained positive for MHC Class II (HLADR; Figure 2b), and were surrounded by $CD4^+$ lymphocytes, suggesting a putative role of $CD20^+$ cells in antigen presentation.[10] Occasional $CD8^+$ cytotoxic T cells and $CD68^+$ macrophages were also seen in the B-cell aggregates. Dense interstitial $CD20^+$ B-cell aggregates[1,2,5] were seen in 53% (17/32) of core biopsy samples with graft rejection. The follicular dendritic cell network as highlighted by CD21 was seen in the $CD20^+$ clusters in 11% of core biopsies (Figure 3a).

$CD38^+$ plasmablasts and plasma cells. Another predominant population of B cells in graft rejection consists of $CD38^+$ plasmablasts and plasma cells. Many of these cells co-segregate with plasma cells, which are positive for CD138 and negative for early B-lineage markers (Figures 1a and 2c). $CD38^+$-rich cellular infiltrates were seen in 59% (19/32) of core biopsies. Many AR biopsies contained both $CD20^+$ clusters and $CD38^+$ B-lineage cells (in 44% (14/32) of core biopsies).

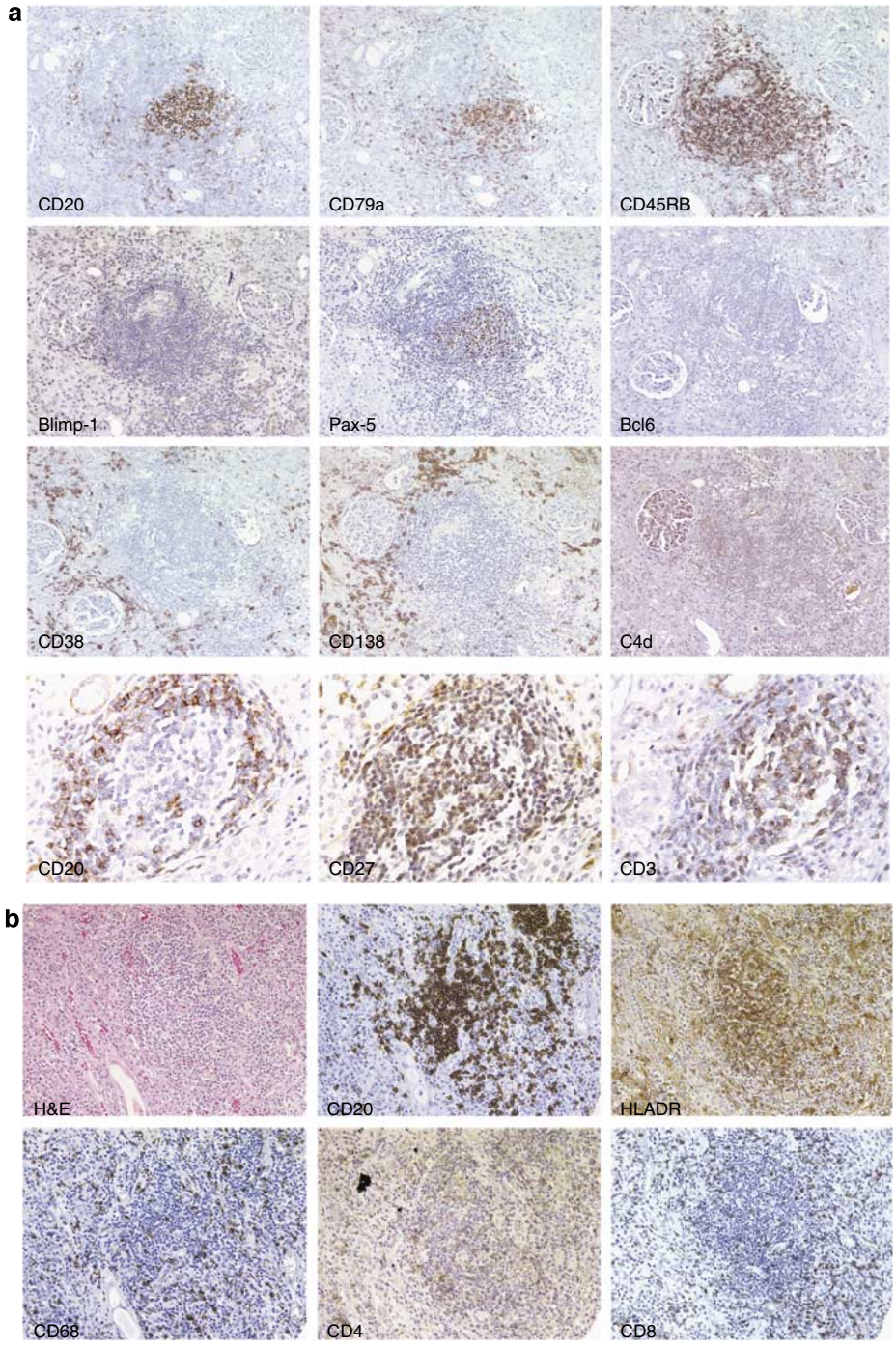

Figure 2 | Characterization of the phenotype of B-cell subsets observed in rejecting K-TMA cores. Multiple immunostains were performed on consecutive K-TMA sections. To localize the B-cell clusters accurately, CD20 immunostains were performed on five different K-TMA sections with other immunostains (mentioned in text) performed on intervening sections. (**a**) Phenotype of $CD20^+$ B-cell clusters in representative T-TMA cores. $CD20^+$ B-cell clusters are also positive for CD79a, CD45RB, and Pax-5, but negative for Blimp-1, Bcl6, CD38, and CD138; C4d stain is negative in this core (original magnification $\times 200$ top panel). These B cells appear to be of early lineage ($Pax\text{-}5^+$) with activated phenotype ($CD79a^+$ and $CD45RB^+$). Representative staining from another core (bottom panel, original magnification $\times 400$) shows that a subset of $CD20^+$ B cells in cluster have a memory B-cell phenotype ($CD27^+$ but $CD3^-$). Some of the $CD27^+$ cells appear to be memory T cells ($CD3^+$ and $CD27^+$). The CD20, CD27, and CD3 stains were performed on consecutive sections. (**b**) Antigen-presenting capacity of $CD20^+$ cells. $CD20^+$ B cells are $HLADR^+$, and are surrounded by $CD4^+$ helper T cells, suggesting a possible B-cell role in antigen presentation. Very few $CD68^+$ and $HLADR^+$ macrophages and dendritic cells are seen in these clusters. A few $CD8^+$ T cells are also seen (original magnification $\times 200$). (**c**) Phenotype of interstitial $CD38^+$ cells. The second B-cell subset consists of late lineage cells, plasmablasts, and plasma cells. These $CD38^+$ areas also stain for CD138, but are negative for CD20, Pax-5 (early B-lineage markers), and CD45RB. A smaller component of $CD79a^+$, $Bcl6^+$, and $Blimp\text{-}1^+$ cells are also seen in these areas. In addition to these B-lineage cells, infiltrating T lymphocytes ($CD3^+$) and macrophages ($CD68^+$) are also seen in these non-clustering interstitial areas. C4d is negative in this K-TMA core (original magnification $\times 200$). On H&E, the $CD38^+$ areas are rich in plasma cells and, in some cases, eosinophils (inset, original magnification $\times 600$).

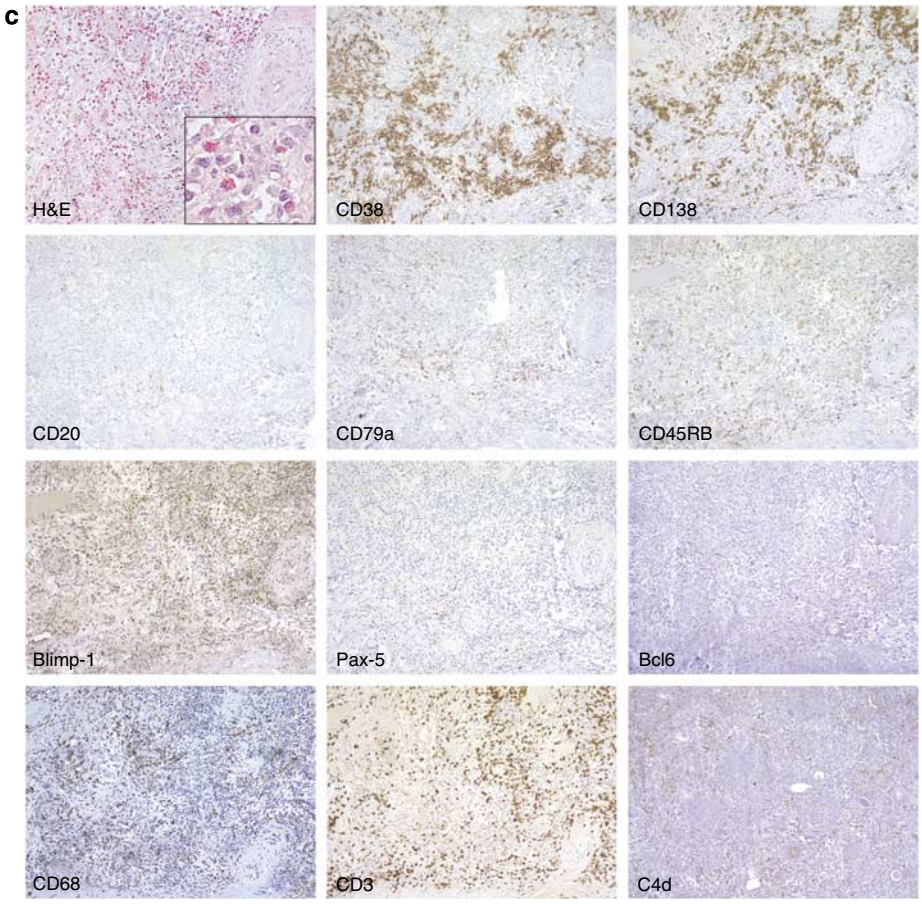

Figure 2 | Continued.

Rejection episodes also had a variable density of infiltrating $CD4^+$ and $CD8^+$ T lymphocytes, $CD68^+$ macrophages, and eosinophils in the interstitium, whereas $CD8^+$ T cells appeared to cause most of the tubulitis. Other cell surface activation markers on infiltrating cells in rejection (CD23 and CD30) were mostly negative (Table S1B).

C4d, donor-specific antibody, and B-cell subsets in graft rejection

C4d stain was scored as positive if seen in peritubular capillaries.[13] $C4d^+$ rejections were noted in 25% (8/32) of core biopsies (Table S2B). Circulating donor-specific antibody (DSA) was detected in 17/26 $C4d^-$ biopsies (65%) and 7/8 of $C4d^+$ core biopsies (88%). Neither C4d nor DSA detection correlated with the presence of $CD20^+$ clusters, as previously reported,[1,2,5] or with $CD138^+$ plasma cells in graft rejection. The presence of circulating DSA correlated strongly with intra-graft CD38 staining ($P=0.01$; $r=0.42$) and weakly with peritubular C4d ($P=0.04$; $r=0.3$) (Table S2B).

Phenotyping infiltrates and chemokines in K-TMA specimens

K-TMA samples had extensive graft rejection and an overarching finding was that the intensity of the infiltrate specific for $CD8^+$ T cells, $CD68^+$ macrophages, $CD20^+$ clusters, and STAT-1 mononuclear cell staining correlated with a strong inflammation score ($P=0.0001$; $r=0.55$). Endothelial cells and infiltrating lymphocytes within $CD20^+$ clusters, as well as $CD38^+$ cells, showed expression for $CXCL12^+$ and VEGF-A. Scattered CXCL13 and CXCR5-positive lymphocytes were seen mainly in $CD20^+$ clusters ($P<0.0001$; $r=0.67$) (Figure 3a),[11,14] as previously published.[11]

A heat-map has been generated for ease of visualization of 27 IHC stains on the 50 K-TMA samples (Figure 3b). On the basis of the similarity of staining scores (see Table S1A and B), a dendrogram on the *x* axis shows that these 50 samples segregate into three groupings or clusters. Cluster-I rejection samples lack CD20 aggregates, but have CD38 and C4d staining, supporting a predominant humoral rejection. Cluster-II rejection samples, despite being nephrectomy samples with AR, have less intense interstitial inflammation; as expected, they segregate with normal K-TMA samples. Cluster-III rejection samples have dense $CD20^+$ infiltrates, as well as $CD38^+$ and C4d, suggesting that these samples may have a mixed, cellular, and humoral rejection.

For the three clusters observed from the K-TMA samples, there were no obvious demographic differences, no

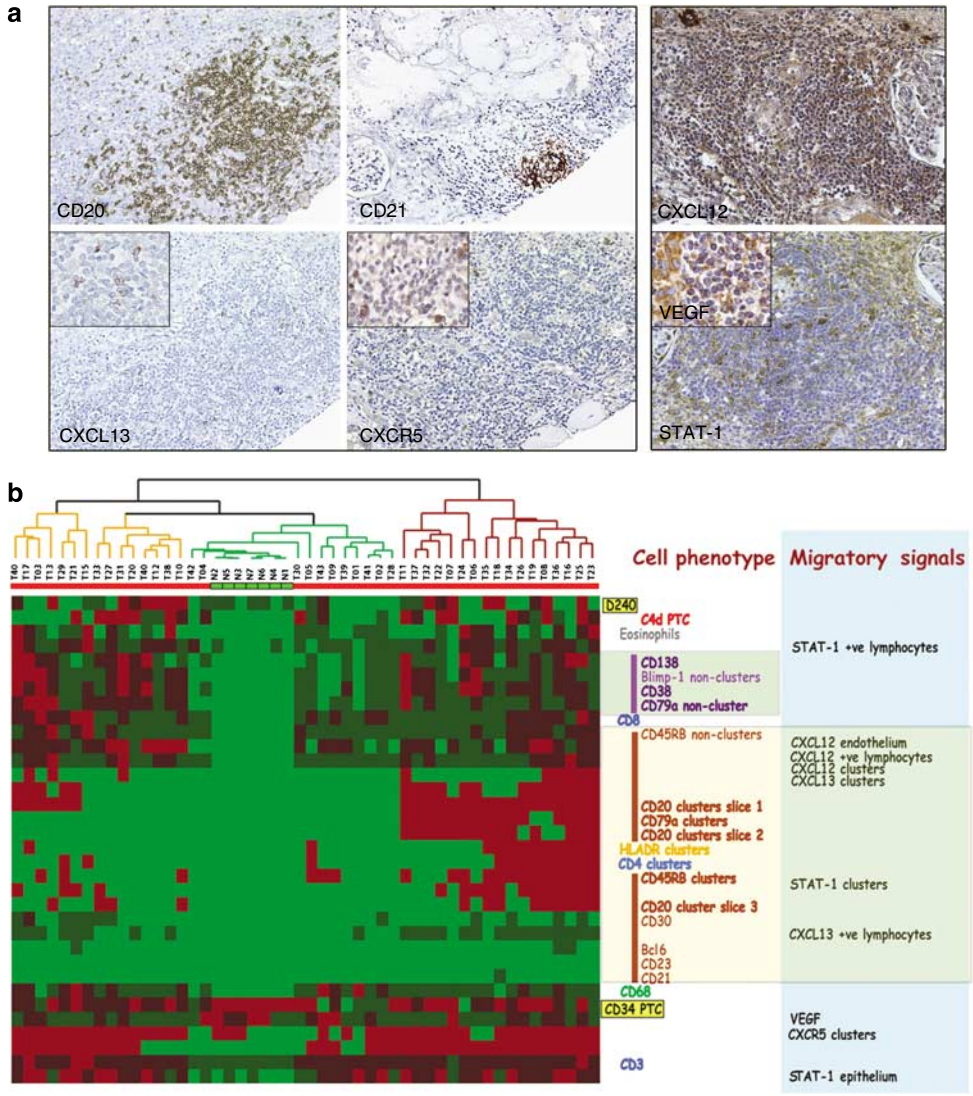

Figure 3 | Putative role of chemokines in modulating the trafficking of B-cell subsets (K-TMA immunostains). (**a**) Signals for the CD20$^+$ cell trafficking. CD20$^+$ B-lymphocyte clusters colocalize rarely with CD21$^+$ follicular dendritic network. A few CXCL13$^+$ and CXCR5$^+$ cells are seen in these clusters as previously published.[11] CD20$^+$ clusters (stain not shown) also co-express CXCL12, VEGF-A, and STAT-1 (right panel, original magnification $\times 200$). (**b**) Cellular infiltrates and trafficking signals in AR visualized by hierarchical clustering of K-TMA immunostains. Fifty nephrectomy specimens utilized for the generation of the K-TMA (Table S1A and B), were stained with 27 individual IHC stains (also see Materials and Methods). As shown here, the individual biopsies are clustered on the *x* axis and the immunostains on the *y* axis. K-TMA samples with rejection are labeled red, K-TMA normal nephrectomy samples are labeled green. Antibody stains were scored semiquantitatively in -2 to 2 scale to allow for variation of stains in a two-color system, with red being maximal at $+2$ and green being minimal at -2. The stains (rows) and samples (columns) are clustered on the basis of the overall similarity in the expression pattern using hierarchical clustering by Cluster, with visualization of data in TreeView.[12] As seen here by the dendrogram on the *x* axis segregating sample similarity, K-TMA samples clustered in three distinct subgroups. Cluster-I (15 samples; T40, 17, 03, 13, 29, 21, 15, 33, 27, 31, 20, 14, 12, 38, and 10) lack CD20$^+$ aggregates, but have severe inflammation (scores 2–3) and prominent accumulation of CD38$^+$ cells. Cluster-III samples (17 samples; T11, 37, 32, 22, 7, 24, 6, 35, 18, 34, 26, 19, 8, 36, 16, 25, and 23) had dense CD20$^+$ aggregates, which were also CD79a$^+$, HLADR$^+$, and segregate with CD4$^+$ T cells, as described in Results. Rejection samples in Cluster-II (T30, 5, 43, 9, 39, 1, 41, 02, 28), colocalizing with normal samples (N1-7) had mild inflammation, fewer infiltrates, and the least tubular atrophy.

differences for recipient/donor age and sex, donor type (living vs deceased), number of previous transplants, days of graft survival, incidence of delayed graft function, antibody titers prior to transplant, HLA mismatches, or the Banff AR grade at the time of nephrectomy.[15,16] Graft survival data were not correlated with K-TMA immunostain results, as graft survival data can be flawed in a K-TMA data set, based on the fact that nephrectomies can often be performed well after complete loss of graft function. On the basis of previously published results, a single correlation analysis was conducted between treatment responsiveness of the AR episode just prior to the nephrectomy, and it was noted that a failure of response to first-line pulse steroid therapy (requiring antibody therapy, that is, 'steroid resistance')

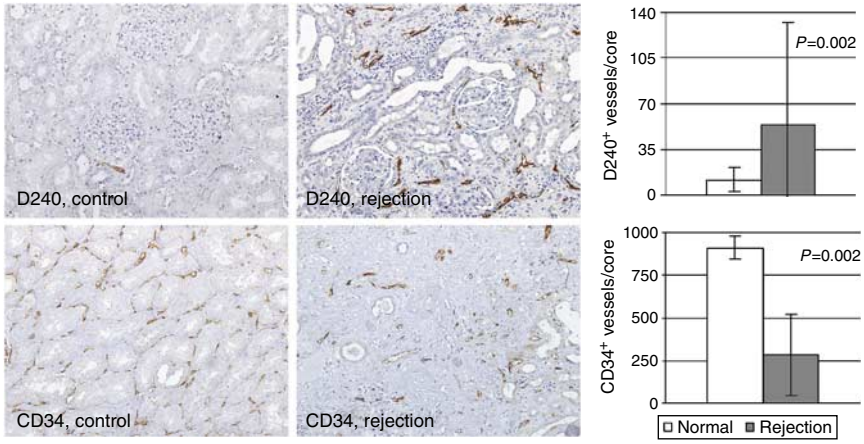

Figure 4 | K-TMA cores with increased number of graft lymphatics (D240$^+$), and reduced microvasculature (CD34$^+$) in AR. K-TMA cores were stained for lymphatic marker D240 as well as endothelial marker CD34 (original magnification $\times$ 200). Left: control normal kidney; right: K-TMA with rejection. The numbers of lymphatics (D240$^+$) and peritubular capillaries (CD34$^+$) per 2 mm core were counted. The number of D240$^+$ vessels was significantly ($P = 0.002$) increased in cases with AR (T1-43) compared with control samples (N1-7). (53.8 ± 78.3 vessels/core in K-TMA AR vs 12 ± 9.5 vessels/core in K-TMA normal samples; $P = 0.002$). Conversely, density of microvasculature, highlighted by CD34$^+$ stain per core was strongly reduced ($P < 0.0001$) with rejection.

occurred more frequently in Cluster-III (the samples with CD20$^+$ cluster infiltrates) compared with Cluster-I (75 vs 27%; $P = 0.007$).

Phenotyping infiltrates in core biopsies, with clinical correlations

On the basis of the most informative K-TMA IHC results, selected immunostains (CD20, CD21, CD38, CD138, CD27, C4d, CD45RB, CD79a, and D240) were performed on core renal allograft biopsies ($n = 37$; 32 Banff-graded AR and 5 stable protocol biopsy controls). Protocol biopsies without graft rejection were negative for all selected immunostains, except positive D240 staining for lymphatics. In biopsies with AR, the density of CD20$^+$ and CD38$^+$ staining, but not C4d$^+$ or Banff AR grade, individually correlated with resistance to steroid therapy. Specifically, steroid resistance was seen in 14/17 CD20$^+$ cases, 15/15 CD38$^+$ biopsies ($P < 0.0001$), and in only 2/8 C4d$^+$ cases. In contrast, only 2/15 CD20$^-$ and 4/17 CD38$^-$ cases were steroid resistant. Intra-graft CD20$^+$ cells were predominantly found in ARs occurring later post transplantation (50 ± 35 months for CD20$^+$ AR vs 22 ± 23 months for CD20$^-$ AR; $P = 0.03$), and, as previously noted, CD20$^+$ graft rejections were at an increased risk of graft loss ($P = 0.0006$; $r = 0.58$; Table S2B). Ten rejection biopsies had graft loss at the current follow-up (Table S2B). CD38 positivity in graft rejection, on the other hand, did not correlate with graft survival.

Non-adherence with immunosuppressive medications appeared to be a major cause of AR in the CD20$^+$ vs the CD20$^-$ group (71 vs 11%; $P = 0.01$) as well as the CD38$^+$ vs the CD38$^-$ group of rejections (73 vs 23%; $P = 0.007$). As expected, patients with graft loss after rejection were more likely to be adolescents (mean age at rejection for patients with graft loss vs no graft loss: 16.7 ± 3.7 vs 12 ± 5.3 years; $P = 0.02$).

Association of vascular and lymphatic markers with B-cell subsets

As B cells have been found to associate with lymphoid neogenesis and lymphangiogenesis,[17–19] whereas endothelial venules and the microvasculature may be specific entry routes for lymphocytes, K-TMA and core biopsies with graft rejection were stained with D240 and CD34, to ascertain any association with the localization of B-cell infiltrates. Gain in lymphatic density, by formation of new lymphatics in the graft, was seen with graft rejection (Figure 4), as previously shown.[20,21] Although lymphangiogenesis was seen in rejection-related lymphocytic infiltrates, including B-cell clusters, it was not specifically associated with B-cell infiltration, did not correlate with time post transplantation or the risk of graft loss following rejection. On the basis of CD34 staining, a reduction of graft microvasculature was seen in graft rejection (Figure 4), with no correlation to B-cell infiltration or time post transplantation.

DISCUSSION

An extensive analysis of acute transplant rejection in human renal allografts has demonstrated that two specific lineages of B cells can form a significant part of the graft infiltrate. Although elucidating the exact role of these cells would require comprehensive cell culture or animal studies, based on existing literature and this extensive study of human biopsies, we can hypothesize about the function of B cells in graft rejection.

CD20$^+$ B-cell clusters, previously identified in graft rejection, appear to consist of activated cells of early B-cell lineage; these cells may have a memory phenotype and express MHC Class II and colocalize with CD4$^+$ T cells. We hypothesize that these B-cell clusters may form follicular dendritic networks and expand into proliferating, antigen-specific CD20$^+$ cells, which survive and can develop a memory phenotype in the presence of continued antigen exposure[22] and persistent

chronic graft inflammation, all likely occurring in rejection episodes resulting from immunosuppression non-adherence. It has been previously shown that chronically inflamed organs can demonstrate ectopic germinal center formation with B-cell activation, and plasma cell differentiation can occur locally.[23,24] However, no definite germinal centers are seen in this data set, limiting the mechanistic hypothesis for the formation and evolution of B-cell clusters in graft rejection. On the basis of the IHC studies and clinical correlates, it is likely that B-cell clusters in rejection can function as efficient antigen-presenting cells, expressing MHC Class II to present processed antigen to CD4 helper T cells, thus driving a C4d-independent, T-cell-dependent cellular rejection, resistant to conventional treatment. It is likely that variations, in part, in the clinical association of $CD20^+$ B-cell clusters and graft outcomes[5,7,8] may be related to differences in the phenotypes of B-cell clusters or differences in the mechanisms of AR escape in these studies. These data are also supported by the K-TMA analysis, which reveals that in Cluster-III, the K-TMA samples with prominent CD20 infiltration during AR, strongly correlates with failure of response to first-line pulse steroid therapy.

Extensive infiltration with $CD38^+$ cells is also seen in graft rejection. CD38 is not entirely specific for cells of plasma cell lineage[25] as it is also expressed on early cells of B and T lineages, NK cells, monocytes, and macrophages. Recognizing this, we have performed sequential stains for B cell, T cell, and macrophage markers, and these studies show that many of the $CD38^+$ cells in graft rejection are plasmablasts and plasma cells. Semiquantitative scoring for $CD38^+$ cells is easier to perform than CD138 staining alone, as CD38 does not have the background tubular epithelial staining of CD138 that makes scoring difficult especially in the setting of tubular atrophy.[26] CD38 has the added advantage of highlighting plasmablasts[27–29] (Figure S5). The lack of significant correlation of CD138 staining with either DSA or C4d in this study may be due to suboptimal semiquantitative scoring for CD138 due to background epithelial staining, and may also relate to the number of biopsies studied.

$CD38^+$ cells (mostly plasmablasts and plasma cells) correlate weakly with intra-graft C4d and very strongly with circulating DSA and may be the progenitor pool for long lived, antibody-producing plasma cells, driving a humoral rejection. The association of an increased incidence of humoral rejection with medication non-adherence, as seen in this study, has also been previously demonstrated.[30] The weak correlation between C4d and DSA seen in our study may be due to possible evanescent nature of C4d staining,[16,31] immunosuppression usage differences, detection methods for C4d,[32] or recipient pediatric age. The loss of microvasculature in AR might also have contributed to the lower incidence of C4d detection (8/32 or 25%) in this study. Thus, CD38 staining may be an alternative IHC marker for detection of antibody-mediated rejection, particularly, in the absence of robust intra-graft C4d staining. It is important to reiterate that the clinical significance of both CD20 and CD38 markers is relevant only in the presence of acute graft rejection, as they can be seen in infiltrates within subcapsular scar, and in the setting of reflux nephropathy and acute pyelonephritis (N Kambham, unpublished data).

B cells are known to induce lymphangiogenesis[17–19] and increased B-cell infiltrates in graft rejection may drive the increased number of observed lymphatics with rejection. It has also been previously suggested that B cells, primed against donor antigen from secondary lymphoid organs, may arrive to the graft from the blood stream through the efferent lymphatics of the secondary lymphoid organs,[20,33] and then exit the graft through newly formed lymphatics. As there is no specific correlation in our study between lymphangiogenesis and the B-cell clusters, some of the B-cell transits into and out of the graft may be occurring by other, undefined mechanisms.

Various chemokines seem to play a role in the movement of and interactions between various lymphocyte subsets; a subset of chemokines in this study were chosen based on their correlation with the B-cell signature in graft rejection[1] (http://sarwal.stanford.edu/Bcell), to investigate if they were specifically associated with B-cell infiltration and clusters. CXCL12 and STAT-1 expression correlated with all infiltrating lymphocytes, including B cells. CXCL12 has been shown to influence the homing of different lymphocytes to the graft, including naive and mature B cells and may also support the persistence of long-lived plasma cells.[34] STAT-1 mediates activation of macrophages and antigen-presenting cells, and stimulates expression of MHC, co-stimulatory, and adhesion molecules,[35,36] on activated T and B cells. CXCL12 appears to be nonspecific chemoattractants for different lymphocyte subsets. VEGF-A, CXCL13, and CXCR5 may support B-cell clusters and B-cell trafficking.[11]

With the observation that this B-cell pool can be seen more often in rejections occurring late post transplantation, it can be postulated that these cells, produced late in the immune response, have a competitive advantage to displace earlier emigrants. These B cells may then be well primed to present antigen to activated T-helper cells and support a robust cellular rejection based on T-cell-dependent B-cell activation. In the absence of therapies directed specifically against this B-cell pool, incomplete treatment of this cellular rejection could be anticipated, resulting in the poor observed transplant outcomes.

Thus, as we discover that various infiltrating cells in the allograft (such as B cells) can have multiple functions, for example, efficient antigen presentation, T-cell activation, antibody production, and secretion of pro-inflammatory cytokines, all dependent on their various stages of differentiation (Figure 5), it is obvious that AR episodes can no longer be considered a generic event. The K-TMA analysis offers some insights into distinct subclasses of AR, weighted by the predominance of certain B-cell infiltrates. An individualized IHC analysis of rejection episodes may be warranted to uncover differing mechanisms supporting and driving rejection injury, so that initial rejection therapy can

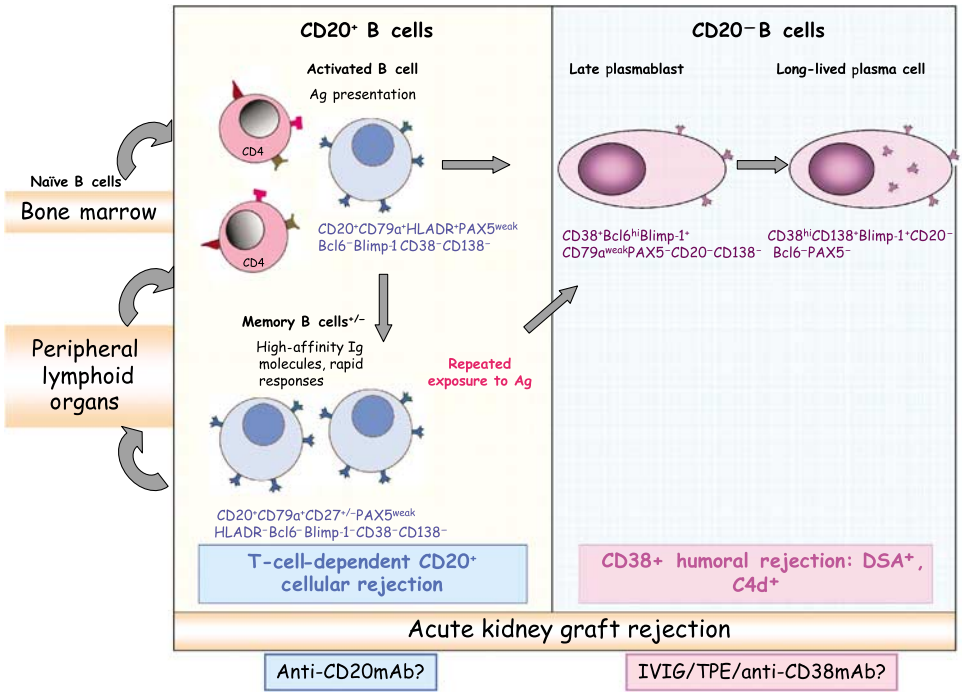

Figure 5 | Summary hypothesis of the phenotype and relevance of B-cell subsets in kidney graft rejection. Naive B cells attain full maturation in the bone marrow and migrate to lymph nodes where antigen presentation occurs. Activated B cells recirculate to the injured graft in rejection through newly formed afferent lymphatics, in response to CXCL13, STAT-1, and VEGF. Recipient-derived $CD20^+$ B cells may efficiently present donor antigen ($HLADR^+$) to primed $CD4^+$ T cells, and, on repeated antigenic exposures, may differentiate into high affinity memory B cells that can persist in the graft in 'ectopic' follicles, supporting a T-cell-dependent cellular rejection. Specific therapeutics depleting $CD20^+$ B cells (such as monoclonal antibody against CD20/Rituximab) may be of benefit. Further differentiation of activated and memory B cells to early and late $CD38^+$ plasmablasts and long-lived plasma cells, result in circulating DSA and humoral rejection. Specific therapies should focus on removal of DSA (intravenous immunoglobulin or TPE/plasmapharesis), and rather than only target $CD20^+$ cells, also consider targeted depletion of $CD38^+$ cells.

be modified and more specifically tailored in a timely manner. Specific characterization of B-cell lineages in rejection could offer unique opportunities for development of targeted rejection therapy. Rituximab, humanized monoclonal antibody against $CD20^+$ cells, has been found to have efficacy against recalcitrant rejection[6,37–40] and may derive its efficacy from its depletion of the B-cell pool, which is persistently presenting antigen. Further studies are required to validate if $CD38^+/CD20^-$ plasmablasts and plasma cells, correlative with DSA levels, could also be a potential marker for humoral rejection. If validated, targeted therapy, such as the development of a monoclonal antibody against CD38 or intravenous immunoglobulin, and plasmapharesis,[41] may be desirable for $CD38^+$ B-cell-rich rejection episodes. Eventually, tailored immunomodulation of rejection episodes may be the critical intervention required for the effective reversal of immunological injury and improved long-term graft survival.

MATERIALS AND METHODS

Tissue and patient information

Histological analyses and IHC stains were performed on K-TMA generated using 2 mm cortex cores from 50 normal ($n=7$) and transplant nephrectomy specimens ($n=43$), as well as on 37 renal allograft 18-gauge needle biopsies from functioning grafts with normal histology ($n=5$; protocol biopsies) and AR ($n=32$). All biopsies were adequate by Banff 1997 Criteria and the presence of AR was determined by established criteria.[15,16] All K-TMA samples had evidence of AR qualified by tubulitis in preserved renal cortex, interstitial inflammation, and presence/absence of vasculitis. The K-TMA was used as a screening tool for the initial, multiple, and sequential IHC stains due to paucity of allograft biopsy material. For details of K-TMA generation, please refer to the web supplement (http://sarwal.stanford.edu/Bcell; Figures S1 and S2). As AR in transplant nephrectomies occurs in the context of markedly reduced or absent immunosuppression, and is thus aggressive and not necessarily the same as rejections seen earlier during the post-transplant course, a subset of 37 patient core biopsies were also chosen for further evaluation of selected, informative K-TMA IHC stains. All the IHC staining procedures performed involved endogenous peroxidase blocking steps as well as the appropriate positive and negative controls, including the use of an isotype-matched immunoglobulin for the latter (Figure S4).

Relevant clinical data were collected on all patients, including date of transplant, type of transplant, HLA match, donor source, donor and recipient age, and immunosuppression (baseline and at rejection). Data were also captured for infection (including protocol measurements of viremia loads for CMV and EBV by peripheral blood quantitative PCR and urinary tract infection), graft function (calculated creatinine clearance by the Schwartz formula[42]), recovery of graft function (defined as return of calculated creatinine clearance to within 10% the baseline pre-AR value, 6 weeks after AR), acute

and chronic rejection grades,[15,16] circulating DSA at rejection, and time to graft loss. Details of the clinical characteristics of the samples used for the K-TMA and the core biopsies are available on the web supplement at Tables S1A and B, and S2A and B, respectively.

Written informed consent was obtained from study patients, and the study was approved by the Institutional Review Board of Stanford University (ID no. 79516 and 75791).

Immunohistochemistry

All slides were stained with H&E (hematoxylin and eosin) and then used for grading AR, chronic graft injury,[15] and for documentation of plasma cells and eosinophils. On K-TMA slides, 27 IHC stains were performed for B-cell lineage (CD20, CD45RB, CD79a, Pax-5, Bcl-6, Blimp-1, CD21, CD23, CD27, CD38, and CD138), T-cell lineage (CD3, CD4, and CD8), macrophages (CD68), HLADR, chemokines and growth factors (CXCL12, CXCL13, CXCR5, VEGF, and STAT-1), endothelial cells (CD34), lymphatics (D240), viral markers (SV40, CMV, and EBV *in situ* hybridization), CD30, and C4d using commercially available antibodies. The following antigens are expressed in various stages of B-cell development: CD20: mature B cells, CD21: follicular dendritic network; CD79a: mature B cells up until plasma cell differentiation, CD27: memory B and T cells, Pax-5: early B cells, Bcl6: germinal center B cells, Blimp-1: mature B cells committed to plasma cell differentiation, CD38: plasmablasts and plasma cells, and CD138: plasma cells.

Selected IHC stains including H&E, CD20, CD38, CD138, CD21, CD27, CD79a, CD45RB, C4d, and D240 were performed on patient core biopsies. B-cell aggregates ($CD20^+$) were defined as dense clusters of B-lymphocytes, measuring >275 cells/h.p.f.[1] Our studies are based on the presence of at least 275 cells/h.p.f. rather than counting the actual number of cells. A $CD20^-$ case has many fewer cells (less than 100 cells/h.p.f.). IHC evidence of infection, lymphoproliferative disorder, or calcineurin inhibitor toxicity was excluded from study. All study patients had negative urine cultures and negative immunostains for CMV, EBV, and polyoma virus (antisera to SV40). The sources of the antibodies and corresponding dilutions are detailed in Table S3.

Semiquantitative histological scoring of K-TMA and core biopsies

Kidney tissue microarray samples. For most stains, slides were scored blindly by a single pathologist (NK) in a semiquantitative manner. The scoring methodology follows previously published TMA scoring systems.[26] Stain scores were calculated on a numerical basis from 0 to 3 based on intensity and extent of staining across individual compartments of renal parenchyma (tubules, glomeruli, vessels, and interstitium) and the infiltrating inflammatory cells. Details of scores generated for each of the stained antibodies are provided in Table S1B. In general, the parenchymal staining was scored as 0, no staining; 1, weak and focal; 2, strong, $<50\%$ of the cortex; 3, strong, $>50\%$ of the cortex; the inflammatory infiltrate was scored as 0, no staining; 1, rare cells; 2, $<30\%$ infiltrate positive; 3, $>30\%$ infiltrate positive. The C4d stain in the peritubular capillaries was scored as $<5\%=0$; 5–20% = 1; 20–50% = 2; $>50\%=3$; glomerular capillary wall staining was also noted. Binary scoring (positive = 1; negative = 0) was used for CD20 and CD38 stains; positive implying dense $CD20^+$ clusters[1] or extensive CD38 staining ($>30\%$ of the infiltrate).

Fluorescence *in situ* hybridization staining

XY chromosome FISH analysis was performed on deparaffinized K-TMA sections (of which 22 were sex mismatched), using probes for X (DXZ1; Spectrum green) and Y (DYZ3; Spectrum orange) chromosomes, and fluorescence was visualized (CytoVision; Applied Imaging, San Jose, CA, USA) using an Olympus BH51 microscope with multiple filters. Results were correlated with H&E and CD20-stained tissue sections. CD20 stain and FISH were performed on consecutive sections to be able to locate the B cells on FISH accurately. Figure 1b–e shows representative staining on a single core (T11) from a male recipient with a female kidney.

Statistical analysis

T-test, Mann–Whitney–Wilcoxon test, χ^2, Fisher's exact, and Jonckheere–Terpstra tests were used for parametric and nonparametric continuous variable and categorical variable comparisons. Two-tailed *P*-value was reported and $P<0.05$ was considered statistically significant. Spearman's and Pearson's correlation coefficients were calculated for clinical outcomes and IHC cell marker stains on the K-TMA and patient core biopsies. All statistical analyses were performed using SAS 9.1.2 (SAS Institute Inc., Cary, NC, USA). Certain results are presented in the format of mean ± standard deviation. Semiquantitative K-TMA immunostaining scores were tabulated with the TMA-Deconvoluter program,[43] converting scores to a -2 to $+2$ normalized scale based on the 0–3 scale ($0=-2$, $1=-1$, $2=1$, and $3=2$) to feed the Cluster program. Hierarchical clustering method was performed by Cluster program[12] to cluster patients and IHC cell marker stains based on centered correlation similarity metrics; the more similar they are, the closer they sit. TreeView program[12] was used to visualize the hierarchical clustering.

Supplementary information

Additional information on methods, clinical information, IHC images, and analytic methods is available in supplementary appendices at http://sarwal.stanford.edu/Bcell.

DISCLOSURE

None of the authors listed have financial interest associated with this work.

ACKNOWLEDGMENTS

MS is funded by 5RO1AI61739-04 for this work.

SUPPLEMENTARY MATERIAL

Figure S1. The K-TMA slide used for this study.
Figure S2. Representative K-TMA cores: 23 out of 28 performed IHC stains on representative 2-mm K-TMA cores of one normal kidney and four transplant nephrectomies.
Figure S3. Presence of memory B and T cells in intra-graft lymphocyte clusters. Two representative 2-mm kidney tissue microarray (K-TMA) cores.
Figure S4. Representative negative control of K-TMA for CXCL13.
Figure S5. Representative CD38-positive biopsy core (C10).
Table S1A. Summary of the clinical characteristics of 43 samples with transplant kidney nephrectomies used in tissue microarray studies.
Table S1B. Clinical and pathological characterization of transplant kidney nephrectomies used in K-TMA and antibody staining score.
Table S2A. Clinical and pathological characterization of biopsy samples from dysfunctional kidneys.
Table S2B. Clinical and pathological characterization of 37 biopsy samples from 28 dysfunctional kidneys and IHC.
Table S3. Antibodies used for IHC staining.
Supplementary material is linked to the online version of the paper at http://www.nature.com/ki

REFERENCES

1. Sarwal M, Chua MS, Kambham N *et al.* Molecular heterogeneity in acute renal allograft rejection identified by DNA microarray profiling. *N Engl J Med* 2003; **349**: 125–138.
2. Hippen BE, DeMattos A, Cook WJ *et al.* Association of $CD20^+$ infiltrates with poorer clinical outcomes in acute cellular rejection of renal allografts. *Am J Transplant* 2005; **5**: 2248–2252.
3. Martins HL, Silva C, Martini D *et al.* Detection of B lymphocytes ($CD20^+$) in renal allograft biopsy specimens. *Transplant Proc* 2007; **39**: 432–434.
4. Krukemeyer MG, Moeller J, Morawietz L *et al.* Description of B lymphocytes and plasma cells, complement, and chemokines/receptors in acute liver allograft rejection. *Transplantation* 2004; **78**: 65–70.
5. Tsai EW, Rianthavorn P, Gjertson DW *et al.* $CD20^+$ lymphocytes in renal allografts are associated with poor graft survival in pediatric patients. *Transplantation* 2006; **82**: 1769–1773.
6. Alausa M, Almagro U, Siddiqi N *et al.* Refractory acute kidney transplant rejection with CD20 graft infiltrates and successful therapy with rituximab. *Clin Transplant* 2005; **19**: 137–140.
7. Bagnasco SM, Tsai W, Rahman MH *et al.* CD20-positive infiltrates in renal allograft biopsies with acute cellular rejection are not associated with worse graft survival. *Am J Transplant* 2007; **7**: 1968–1973.
8. Kayler LK, Lakkis FG, Morgan C *et al.* Acute cellular rejection with CD20-positive lymphoid clusters in kidney transplant patients following lymphocyte depletion. *Am J Transplant* 2007; **7**: 949–954.
9. Doria C, di Francesco F, Ramirez CB *et al.* The presence of B-cell nodules does not necessarily portend a less favorable outcome to therapy in patients with acute cellular rejection of a renal allograft. *Transplant Proc* 2006; **38**: 3441–3444.
10. Noorchashm H, Reed AJ, Rostami SY *et al.* B cell-mediated antigen presentation is required for the pathogenesis of acute cardiac allograft rejection. *J Immunol* 2006; **177**: 7715–7722.
11. Steinmetz OM, Panzer U, Kneissler U *et al.* BCA-1/CXCL13 expression is associated with CXCR5-positive B-cell cluster formation in acute renal transplant rejection. *Kidney Int* 2005; **67**: 1616–1621.
12. Eisen MB, Spellman PT, Brown PO *et al.* Cluster analysis and display of genome-wide expression patterns. *Proc Natl Acad Sci USA* 1998; **95**: 14863–14868.
13. Colvin RB, Smith RN. Antibody-mediated organ-allograft rejection. *Nat Rev Immunol* 2005; **5**: 807–817.
14. Grogg KL, Attygalle AD, Macon WR *et al.* Expression of CXCL13, a chemokine highly upregulated in germinal center T-helper cells, distinguishes angioimmunoblastic T-cell lymphoma from peripheral T-cell lymphoma, unspecified. *Mod Pathol* 2006; **19**: 1101–1107.
15. Racusen LC, Solez K, Colvin RB *et al.* The Banff 97 working classification of renal allograft pathology. *Kidney Int* 1999; **55**: 713–723.
16. Racusen LC, Colvin RB, Solez K *et al.* Antibody-mediated rejection criteria—an addition to the Banff 97 classification of renal allograft rejection. *Am J Transplant* 2003; **3**: 708–714.
17. Angeli V, Ginhoux F, Llodra J *et al.* B cell-driven lymphangiogenesis in inflamed lymph nodes enhances dendritic cell mobilization. *Immunity* 2006; **24**: 203–215.
18. Martin F, Chan AC. Pathogenic roles of B cells in human autoimmunity; insights from the clinic. *Immunity* 2004; **20**: 517–527.
19. Martin F, Chan AC. B cell immunobiology in disease: evolving concepts from the clinic. *Annu Rev Immunol* 2006; **24**: 467–496.
20. Kerjaschki D, Regele HM, Moosberger I *et al.* Lymphatic neoangiogenesis in human kidney transplants is associated with immunologically active lymphocytic infiltrates. *J Am Soc Nephrol* 2004; **15**: 603–612.
21. Stuht S, Gwinner W, Franz I *et al.* Lymphatic neoangiogenesis in human renal allografts: results from sequential protocol biopsies. *Am J Transplant* 2007; **7**: 377–384.
22. Tarlinton D. B-cell memory: are subsets necessary? *Nat Rev Immunol* 2006; **6**: 785–790.
23. Cassese G, Lindenau S, de Boer B *et al.* Inflamed kidneys of NZB/W mice are a major site for the homeostasis of plasma cells. *Eur J Immunol* 2001; **31**: 2726–2732.
24. Magalhaes R, Stiehl P, Morawietz L *et al.* Morphological and molecular pathology of the B cell response in synovitis of rheumatoid arthritis. *Virchows Arch* 2002; **441**: 415–427.
25. Mehta K, Shahid U, Malavasi F. Human CD38, a cell-surface protein with multiple functions. *FASEB J* 1996; **10**: 1408–1417.
26. Kambham N, Kong C, Longacre TA *et al.* Utility of syndecan-1 (CD138) expression in the diagnosis of undifferentiated malignant neoplasms: a tissue microarray study of 1,754 cases. *Appl Immunohistochem Mol Morphol* 2005; **13**: 304–310.
27. Campana D, Suzuki T, Todisco E *et al.* CD38 in hematopoiesis. *Chem Immunol* 2000; **75**: 169–188.
28. Pers JO, Devauchelle V, Daridon C *et al.* BAFF-modulated repopulation of B lymphocytes in the blood and salivary glands of rituximab-treated patients with Sjogren's syndrome. *Arthritis Rheum* 2007; **56**: 1464–1477.
29. Avery DT, Ellyard JI, Mackay F *et al.* Increased expression of CD27 on activated human memory B cells correlates with their commitment to the plasma cell lineage. *J Immunol* 2005; **174**: 4034–4042.
30. Lerut E, Kuypers DR, Verbeken E *et al.* Acute rejection in non-compliant renal allograft recipients: a distinct morphology. *Clin Transplant* 2007; **21**: 344–351.
31. Nickeleit V, Zeiler M, Gudat F *et al.* Detection of the complement degradation product C4d in renal allografts: diagnostic and therapeutic implications. *J Am Soc Nephrol* 2002; **13**: 242–251.
32. Seemayer CA, Gaspert A, Nickeleit V *et al.* C4d staining of renal allograft biopsies: a comparative analysis of different staining techniques. *Nephrol Dial Transplant* 2007; **22**: 568–576.
33. Kerjaschki D. Lymphatic neoangiogenesis in renal transplants: a driving force of chronic rejection? *J Nephrol* 2006; **19**: 403–406.
34. Ellyard JI, Avery DT, Mackay CR *et al.* Contribution of stromal cells to the migration, function and retention of plasma cells in human spleen: potential roles of CXCL12, IL-6 and CD54. *Eur J Immunol* 2005; **35**: 699–708.
35. Hollenbaugh D, Mischel-Petty N, Edwards CP *et al.* Expression of functional CD40 by vascular endothelial cells. *J Exp Med* 1995; **182**: 33–40.
36. Carlos TM, Harlan JM. Leukocyte–endothelial adhesion molecules. *Blood* 1994; **84**: 2068–2101.
37. Lehnhardt A, Mengel M, Pape L *et al.* Nodular B-cell aggregates associated with treatment refractory renal transplant rejection resolved by rituximab. *Am J Transplant* 2006; **6**: 847–851.
38. Faguer S, Kamar N, Guilbeaud-Frugier C *et al.* Rituximab therapy for acute humoral rejection after kidney transplantation. *Transplantation* 2007; **83**: 1277–1280.
39. Becker YT, Becker BN, Pirsch JD *et al.* Rituximab as treatment for refractory kidney transplant rejection. *Am J Transplant* 2004; **4**: 996–1001.
40. Genberg H, Hansson A, Wernerson A *et al.* Pharmacodynamics of rituximab in kidney allotransplantation. *Am J Transplant* 2006; **6**: 2418–2428.
41. Jordan SC, Quartel AW, Czer LS *et al.* Posttransplant therapy using high-dose human immunoglobulin (intravenous gammaglobulin) to control acute humoral rejection in renal and cardiac allograft recipients and potential mechanism of action. *Transplantation* 1998; **66**: 800–805.
42. Schwartz GJ, Haycock GB, Edelmann Jr CM *et al.* A simple estimate of glomerular filtration rate in children derived from body length and plasma creatinine. *Pediatrics* 1976; **58**: 259–263.
43. Liu CL, Prapong W, Natkunam Y *et al.* Software tools for high-throughput analysis and archiving of immunohistochemistry staining data obtained with tissue microarrays. *Am J Pathol* 2002; **161**: 1557–1565.